


Upper Limit of Sound Speed in Nuclear Matter: A Harmonious Interplay of Transport Calculation and Perturbative QCD Constraint

SHAO-PENG TANG ¹, YONG-JIA HUANG ^{1,2}, MING-ZHE HAN ^{1,3} AND YI-ZHONG FAN ^{1,4}

¹Key Laboratory of Dark Matter and Space Astronomy, Purple Mountain Observatory, Chinese Academy of Sciences, Nanjing 210033, China

²RIKEN Interdisciplinary Theoretical and Mathematical Sciences Program (iTHEMS), RIKEN, Wako 351-0198, Japan

³Max-Planck-Institut für Gravitationsphysik (Albert-Einstein-Institut), Am Mühlenberg 1, D-14476 Potsdam-Golm, Germany

⁴School of Astronomy and Space Science, University of Science and Technology of China, Hefei, Anhui 230026, China

(Received ...; Revised ...; Accepted ...; Published ...)

ABSTRACT

Very recently, it has been shown that there is an upper bound on the squared sound speed of nuclear matter from the transport, which reads $c_s^2 \leq 0.781$ (Hippert et al. 2024). In this work, we demonstrate that this upper bound is corroborated by the reconstructed equation of state (EOS; modeled with a nonparametric method) for ultra-dense matter. The reconstruction integrates multi-messenger observation for neutron stars (NSs), in particular, the latest radius measurements for PSR J0437–4715 ($11.36_{-0.63}^{+0.95}$ km), PSR J0030+0451 ($11.71_{-0.83}^{+0.88}$ km, in the ST+PDT model), and PSR J0740+6620 ($12.49_{-0.88}^{+1.28}$ km) by NICER have been adopted. The result shows in all cases, the $c_s^2 \leq 0.781$ upper limit for EOS will naturally yield the properties of matter near center of the massive neutron star consistent with the causality-driven constraint from pQCD, where in practice, the constraint is applied at ten nuclear saturation density ($n_L = 10n_s$). We also note that there is a strong correlation for the maximum c_s^2 with n_L , and $c_s^2 \leq 0.781$ is somehow violated when $n_L = n_{c,\text{TOV}}$. The result indicates that a higher density in implementing the pQCD constraint, even considering the uncertainties from statistics, is more natural. Moreover, the remarkable agreement between the outcomes derived from these two distinct and independent constraints (i.e., the transport calculation and pQCD boundary) lends strong support to their validity. Besides, the latest joint constraint for $R_{1.4}$, $R_{2.0}$, $R_{1.4} - R_{2.0}$, and M_{TOV} are $11.94_{-0.68}^{+0.77}$ km, $11.99_{-0.67}^{+0.88}$ km, $-0.1_{-0.27}^{+0.42}$ km, and $2.24_{-0.10}^{+0.13} M_\odot$ (at 90% credible level), respectively.

1. INTRODUCTION

The observation of neutron stars (NSs) with masses surpassing $2M_\odot$ (Antoniadis et al. 2013; Fonseca et al. 2021) implies that the speed of sound must exceed the conformal limit at certain densities (Bedaque & Steiner 2015) and the speed of sound (as a function of density) within the neutron star EOS is believed to be nonmonotonic, characterized by the presence of at least one peak (Annala et al. 2020; Altiparmak et al. 2022; Gorda et al. 2023; Han et al. 2023; Jiang et al. 2023; Yao et al. 2023). This has raised the general theoretical question – how high can the speed of sound be within physically plausible systems or theories? In a recent study, Hippert et al.

(2024) summarized the transport coefficients for nuclear matter in many theories (Policastro et al. 2001; Baier et al. 2008; Romatschke & Romatschke 2007; Moore & Sohrabi 2012; Arnold et al. 2003; Romatschke & Romatschke 2017), and found they would finally yield an upper limit of $c_s^2 \leq 0.781$ for all known systems. It is however noted that in principle, this bound could be surpassed in some ideal systems (Moore 2024). In this work, with the information from various direction, we show that the constraint for nuclear matter sound speed will naturally lead to the properties of matter near the center of the most massive NS well consistent with the causality-driven constraint from perturbative quantum chromodynamic (pQCD).

Advancements in pQCD calculations have garnered significant interest due to their contributions in bounding the neutron star (NS) EOS (Annala et al. 2020; Alt-

parmak et al. 2022; Komoltsev & Kurkela 2022; Kurkela 2022; Gorda et al. 2023; Han et al. 2023; Brandes et al. 2023a,b; Mroczek et al. 2023; Somasundaram et al. 2023; Zhou 2023; Komoltsev et al. 2023; Fan et al. 2024; Vuorinen 2024). Given the challenge of inferring the state of matter in the vicinity of the NS core from observable NS properties, the incorporation of insights from pQCD is essential for achieving a more rigorous constraint on the EOS. Although the perturbative calculation is only valid in ultra-high density, such boundary conditions could be extended to lower chemical potential based on thermodynamic stability and causality. As a result, soft cores are generally required in massive NS. However, it is still in debate, one reason is whether the soft core is required somehow depends upon the density to implement the causality-driven constraint from pQCD. Various studies have examined the density at which pQCD constraints should be implemented, with no consensus reached thus far (Somasundaram et al. 2023; Gorda et al. 2023; Essick et al. 2023; Zhou 2023; Fan et al. 2024).

In this work, we study the NS EOS and its sound speed by using the multi-messenger observations and the theoretical constraint. We incorporate all of the information with Bayesian inference, while the Gaussian-process EOS generator guarantees the method is non-parametric. We examine how the upper bound of c_s^2 affects the EOS of ultradense matter and demonstrate that the maximal values of c_s^2 , derived from multi-messenger neutron star (NS) observations and pQCD constraints that applied at $n_L = 10n_s$ (where n_s is the nuclear saturation density), are in good agreement with the theoretical upper bound of $c_s^2 \leq 0.781$. However, this upper bound is partially violated when pQCD constraints are imposed at $n_L = n_{c,\text{TOV}}$, the central density of the maximum mass NS configuration. These results provide support for the application of pQCD constraints at densities surpassing those found within NSs, potentially leading to a more precise understanding of the EOS for NSs and the behavior of matter under extreme conditions. Moreover, by applying the transport upper bound on the constructed EOS but without pQCD information, we can corroborate many projections predicted on pQCD constraints at $10n_s$. The concordance observed between these different physical models mutually reinforces their validity.

2. METHODS

Building upon the methodology delineated in our previous works (Tang et al. 2024) (see also Gorda et al. 2023 and Fan et al. 2024), we implement the Gaussian Process (GP) method (Landry & Essick 2019; Essick et al. 2020; Landry et al. 2020) to generate an ensemble

of EOS. The posterior distribution of the EOS is constructed by selecting samples based on their likelihoods, denoted as $\mathcal{L} = \mathcal{L}_{\text{GW}} \times \mathcal{L}_{\text{NICER}} \times \mathcal{L}_{\text{Mmax}} \times \mathcal{L}_{\text{pQCD}}$. Here, \mathcal{L}_{GW} quantifies the likelihood associated with the mass-tidal deformability measurements from GW170817 (Abbott et al. 2018, 2019), and $\mathcal{L}_{\text{NICER}}$ corresponds to the likelihood of NICER observations, specifically the latest mass and/or radius measurements for PSR J0030+0451 (i.e., the ST+PDT model results reported in Vinciguerra et al. (2024), since the PDT-U model is disfavored (Luo et al. 2024)), PSR J0740+6620 (Salmi et al. 2024; Dittmann et al. 2024), and PSR J0437–4715 ($R_{1.418M_\odot} = 11.36^{+0.95}_{-0.63}$ km at the 68.3% credible level¹ (Choudhury et al. 2024)). The term $\mathcal{L}_{\text{Mmax}}$ is the marginalized posterior distribution of the maximum mass cutoff for NSs, as adopted from Fan et al. (2024). Lastly, $\mathcal{L}_{\text{pQCD}} = \mathcal{P}(n_L, \varepsilon(n_L, \text{EOS}), p(n_L, \text{EOS}))$ represents the likelihood of the pQCD constraints at a density of n_L (Komoltsev & Kurkela 2022; Gorda et al. 2023), where ε and p denote the energy density and pressure, respectively. In this study, we examine the implications of applying pQCD constraints in two distinct scenarios: one where the constraints are imposed at the core density corresponding to the maximum mass of non-rotating NSs, and another at a density of $n_L = 10n_s$. The extension of pQCD to lower densities, such as $10n_s$, involves the consideration of two distinct upper limits for the squared speed of sound. The first upper limit is based on the principle of causality and is represented as $\text{pQCD}(10n_s, c_s^2 \leq 1)$, while the second is derived from transport and is denoted as $\text{pQCD}(10n_s, c_s^2 \leq 0.781)$. Furthermore, we explore the implications of applying a c_s^2 upper limit that is applicable to the entire EOS, extending to densities well beyond that of a NS, and is specified as $c_s^2(n \leq 40n_s) \leq 0.781$. This investigation is conducted without including the pQCD likelihood term.

3. RESULTS

As depicted in the top panel of Figure 1, the square of the speed of sound, $c_s^2(n)$, is reconstructed utilizing multimessenger NS observations in conjunction with the constraints of pQCD at a density of $n_L = n_{c,\text{TOV}}$. We find that the reconstructed c_s^2 exhibits subconformality ($c_s^2 \leq 1/3$) at low densities and there is a rapid increase in the value of c_s^2 as the density increases from $1.5n_s$ to $3n_s$. Beyond $3n_s$, the 90% upper limit for c_s^2 surpasses the transport bound of $c_s^2 \leq 0.781$, suggesting that either the pQCD constraints applied at $n_L = n_{c,\text{TOV}}$ is not

¹ Intriguingly, this radius measurement is well consistent with that of PSR J0030+0451 in the ST+PDT model (Vinciguerra et al. 2024).

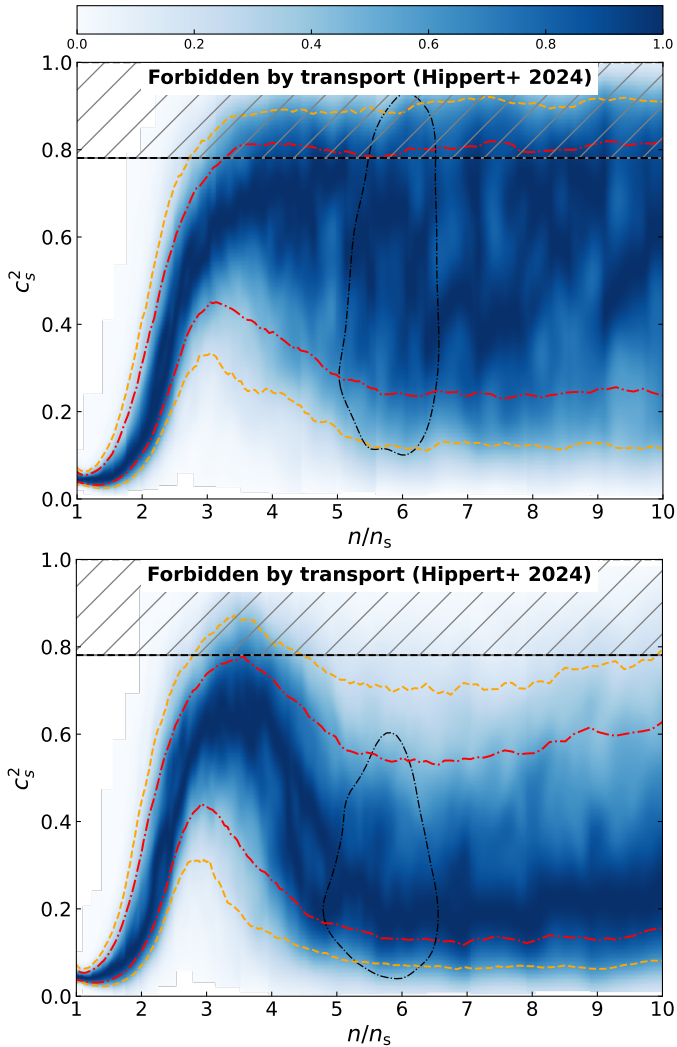


Figure 1. Density distribution of the sound speed squared (c_s^2) as a function of the number density n normalized to n_s . Top panel: This result is derived using $n_L = n_{c,\text{TOV}}$. The red dash-dotted and orange dashed curves represent the 68.3% and 90% confidence regions, respectively. The transport bound $c_s^2 \leq 0.781$ (Hippert et al. 2024) is delineated by a hatched pattern and labeled as “Forbidden by transport.” Additionally, the black dash-dotted line indicates the 68.3% contour for $n_{c,\text{TOV}}$ and its associated values of c_s^2 . Bottom panel: The same as top panel, but is derived using $n_L = 10n_s$. The results in both panels are obtained with $c_s^2 \leq 1$ extension of pQCD to lower densities.

supported or that the matter composition beyond $3.5n_s$ potentially deviates from ‘ordinary’ nuclear matter. At densities above $5n_s$, the constraints on c_s^2 become significantly less stringent due to the reduced informativeness of multimessenger data and the very weak influence of the pQCD constraint with $n_L = n_{c,\text{TOV}}$.

Upon implementing pQCD constraints at a density of $n_L = 10n_s$, the EOS within the density range of $1.5n_s$

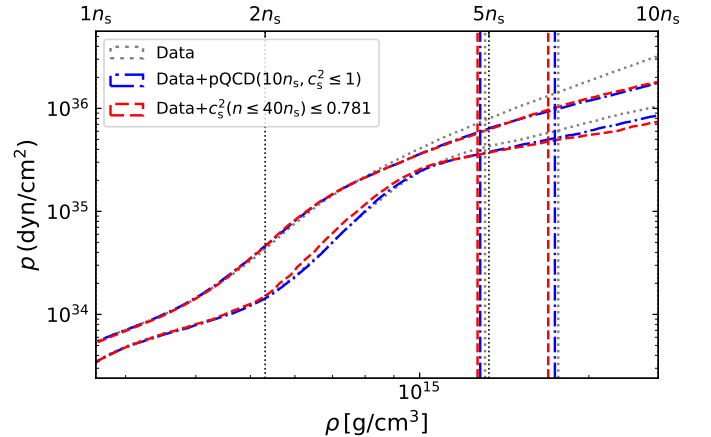


Figure 2. Reconstructed 90% credible regions for the pressure versus rest-mass density relationship. The grey dotted lines represent the results derived from multimessenger NS observations. The blue and red lines correspond to results obtained when additional constraints from pQCD are imposed at density of $10n_s$, and when incorporating additional transport upper bound of $c_s^2 \leq 0.781$, respectively.

to $3n_s$ exhibits a similar stiffness to that observed when $n_L = n_{c,\text{TOV}}$. However, at densities exceeding $3.5n_s$, the squared speed of sound decreases rapidly, exhibiting a pronounced peak at $3.5n_s$, with a magnitude in agreement with the transport bound, as depicted in the bottom panel of Figure 1. This phenomenon is primarily attributed to the stiffening of the EOS required to support NSs with masses surpassing $2M_\odot$ (Antoniadis et al. 2013; Fonseca et al. 2021) and the softening of the EOS by pQCD constraints. In contrast to the $n_L = n_{c,\text{TOV}}$ scenario, the sound speed at $n_{c,\text{TOV}}$ is more likely to fall below the conformal limit. This suggests that the core of a maximum mass NS may contain matter that deviates from pure hadronic compositions. Across higher density regions, the c_s^2 values roughly distributed around approximately 0.2, a result attributed to the pQCD constraint applied at large density (e.g., $n_L \geq 10n_s$). We also observe that the majority of the $c_s^2(n)$ results across the entire density range adhere to the established upper limit of c_s^2 as informed by nuclear matter transport calculations. The extension of pQCD to lower densities is contingent upon the upper bound of the speed of sound squared. We have verified that employing an upper limit of $c_s^2 \leq 0.781$ does not affect the outcomes derived from causal extrapolation. For additional details, please refer to the supplementary material.

Below, we assess the consistency between the transport calculations and the pQCD constraints applied at densities of $n_L = 10n_s$. We establish an upper bound for the speed of sound squared, c_s^2 , within the proposed EOS based on transport calculation (Hippert et al. 2024).

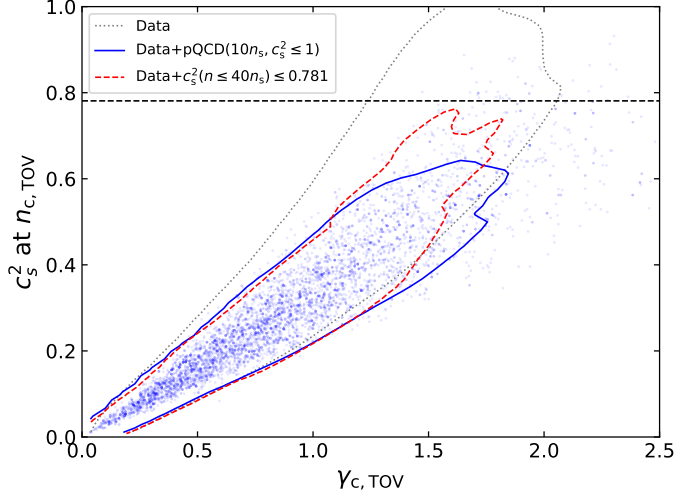


Figure 3. The properties (c_s^2 vs. γ) of the matter at the center of the most massive non-rotating NS. The grey dotted lines represent the results derived from multimessenger NS observations. The blue and red lines correspond to results (90% credibility) obtained for the pQCD constraint imposed at $n_L = 10n_s$, and for the additional transport upper bound of $c_s^2 \leq 0.781$.

This bounded-EOS results are then compared with the results derived from pQCD constraints at $n_L = 10n_s$, which incorporate causality extrapolation. As shown in Figure 2, there is a remarkable agreement between these two approaches (refer to the Supplementary Material for results normalized to $n_{c,\text{TOV}}$). Additionally, both methodologies indicate a softening of the EOS at higher densities compared to that obtained with only multimessenger observations of NSs. The central state of the most massive non-rotating NS, characterized by the squared speed of sound (c_s^2) and the polytropic index ($\gamma_{c,\text{TOV}}$), demonstrates significant uniformity. The maximum mass (M_{TOV}) and corresponding radius (R_{TOV}) of a non-rotating NS have been demonstrated to be crucial in probing the high-density EOS (Tang et al. 2024). We find that there is a remarkable consistency in these critical macroscopic properties of NSs when comparing results obtained with the transport bound to those constrained by pQCD, which also validates the M_{TOV} found in Fan et al. (2024). Similarly, the mass-radius relationships also exhibit notable consistency, as detailed in the Supplementary Material.

We have examined the ‘typical’ densities at which pQCD constraints are applied, specifically $n_{c,\text{TOV}}$ and $10n_s$. It has become apparent that the maximum values of c_s^2 within NSs—denoted as $c_{s,\text{max}}^2(n \leq n_{c,\text{TOV}})$ —vary between these two scenarios. Consequently, our aim is to elucidate the general trend or relationship between $c_{s,\text{max}}^2(n \leq n_{c,\text{TOV}})$ and the densities at which pQCD

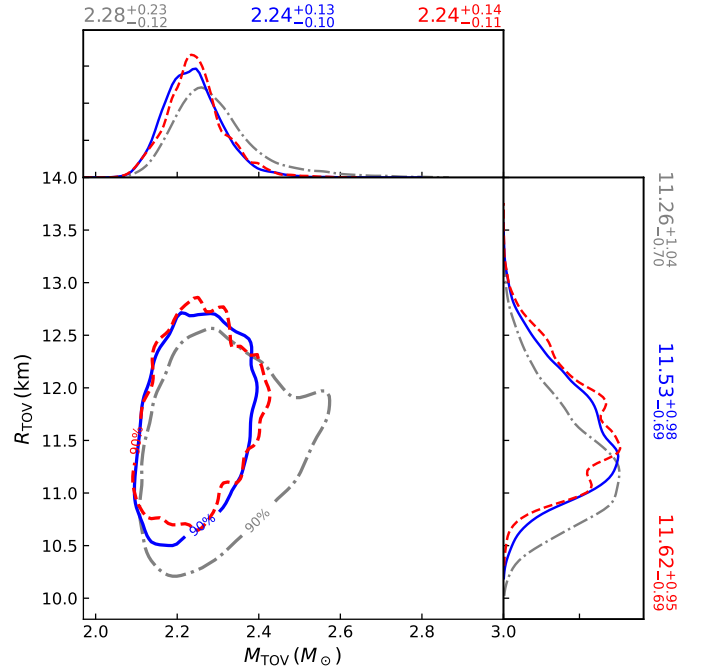


Figure 4. Posterior distributions of M_{TOV} and R_{TOV} (90% credibility). The grey dash-dotted lines represent the results derived from multimessenger NS observations. The blue and red lines correspond to results obtained when additional constraints from pQCD are imposed at density of $10n_s$, and when incorporating additional transport upper bound of $c_s^2 \leq 0.781$, respectively.

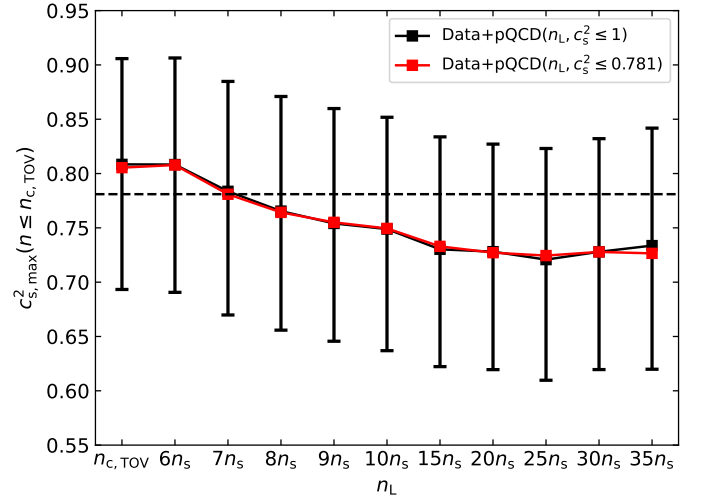


Figure 5. Correlation between the applied densities of pQCD constraints and the corresponding maximal values of c_s^2 within NS. The black 1σ error bar represents the results derived from extrapolating pQCD constraints to lower densities with causality. In contrast, the red line represents the results for the extension with $c_s^2 \leq 0.781$.

constraints are applied, which we denote as n_L . As depicted in Figure 5, a negative correlation between these two variables is observed. With the increment of n_L , the value of $c_{s,\max}^2$ ($n \leq n_{c,\text{TOV}}$) exhibits a gradual decrease until it approaches approximately $15n_s$, beyond which it remains nearly constant. This intriguing pattern offers a novel approach to probing the appropriate densities for the application of pQCD constraints. Given that such densities are not directly observable, the maximum values of c_s^2 within NSs can be indirectly constrained through astrophysical observations (Ecker & Rezzolla 2022). The result also suggests that a higher density in implementing the pQCD constraint, even considering the uncertainties from statistics, is more natural.

4. SUMMARY AND DISCUSSION

Prior research has established that the sound speed must surpass the conformal limit at certain densities to sustain observations of massive NSs (Bedaque & Steiner 2015; Reed & Horowitz 2020; Han et al. 2023; Tang et al. 2024). The speed of sound (as a function of density) within the neutron star EOS is believed to be nonmonotonic, characterized by the presence of at least one peak. The minimum of this peak is presumed to coincide with the conformal limit. A recent study by Hippert et al. (2024) proposes that the square of the sound speed is subject to an upper limit, derived from nuclear matter transport calculations, while it is still in debate (Moore 2024). Determining whether there exists a more stringent or readily attainable upper limit than that imposed by causality in nature is a compelling avenue for further study. In this study, the new radius measurements for PSR J0437–4715 ($11.36_{-0.63}^{+0.95}$ km), PSR J0030+0451 ($11.71_{-0.83}^{+0.88}$ km, in the ST+PDT model), and PSR

J0740+6620 ($12.49_{-0.88}^{+1.28}$ km) have been adopted. We find that multimessenger NS observations, when combined with pQCD constraints applied at high densities (e.g., $n \geq 10n_s$) lead to an upper bound on c_s^2 , which is consistent with the bound from transport calculations. Additionally, we identify a negative correlation between n_L and the $c_{s,\max}^2$ that may become observable with future multimessenger observations. Therefore, it is more natural to consider a higher n_L for pQCD constraint. We have examined the robustness of the above results against previous radius measurement for PSR J0030+0451 (Riley et al. 2019; Miller et al. 2019). The new estimation for $R_{1.4}$ is smaller than the earlier reported value, resulting in a marginally higher maximum c_s^2 inside NS (see also the appendix of Fan et al. (2024)), while the consistency is still hold. Moreover, if the upper bound by transport is assumed to be valid across the entire EOS, it also reproduces many predictions derived from pQCD constraints, including the pressure-density and the NS mass-radius relationships. This suggests that these two distinctly different approaches—pQCD and transport calculations—converge on the same conclusion. Such convergence hints at a profound underlying similarity in the fundamental properties of nature.

- 1 This work is supported by the National Natural Science Foundation of China under Grants No. 12233011
- 2 and No. 12303056, the Project for Special Research
- 3 Assistant and the Project for Young Scientists in Basic Research (No. YSBR-088) of the Chinese Academy
- 4 of Sciences, the General Fund (No. 2023M733735, No.
- 5 2023M733736) of the China Postdoctoral Science Foundation (CPSF), and the Postdoctoral Fellowship Program of CPSF (GZB20230839, GZC20241915).

APPENDIX

In the main text, we have examined the effect of varying the densities n_L at which the perturbative Quantum Chromodynamics (pQCD) is applied. Specifically, we focus on the densities $n_L = n_{c,\text{TOV}}$ and $n_L = 10n_s$. These variations significantly influence the structure of the $c_s^2 - n$ relationship. The findings discussed are predicated on an extension of pQCD to lower densities that adheres to the principle of causality. Here we provide complementary results derived from extending pQCD to lower densities while adhering to the transport upper bound. As illustrated in Figure 6, the outcomes are nearly identical to those previously reported.

In the main text, we have presented a comparison of the pressure versus rest-mass density relationships derived from the imposition of a transport upper bound to c_s^2 and that obtained under the constraints of pQCD applied at $n_L = 10n_s$. Here we normalize the pressure versus number density results to the central density of a maximally massive non-rotating NS, $n_{c,\text{TOV}}$. These normalized results also demonstrate consistent agreement across the different methodologies employed. We further examine the consistency of the mass-radius relationship. As depicted in Figure 8, the findings from both approaches are in agreement and conform well to the observational data for NSs.

Finally, we present the distributions of some key parameters. Figure 9 depicts the probability distributions for the maximum mass (M_{TOV}) and corresponding radius (R_{TOV}) of a non-rotating NS, along with the radius ($R_{1.4}$)

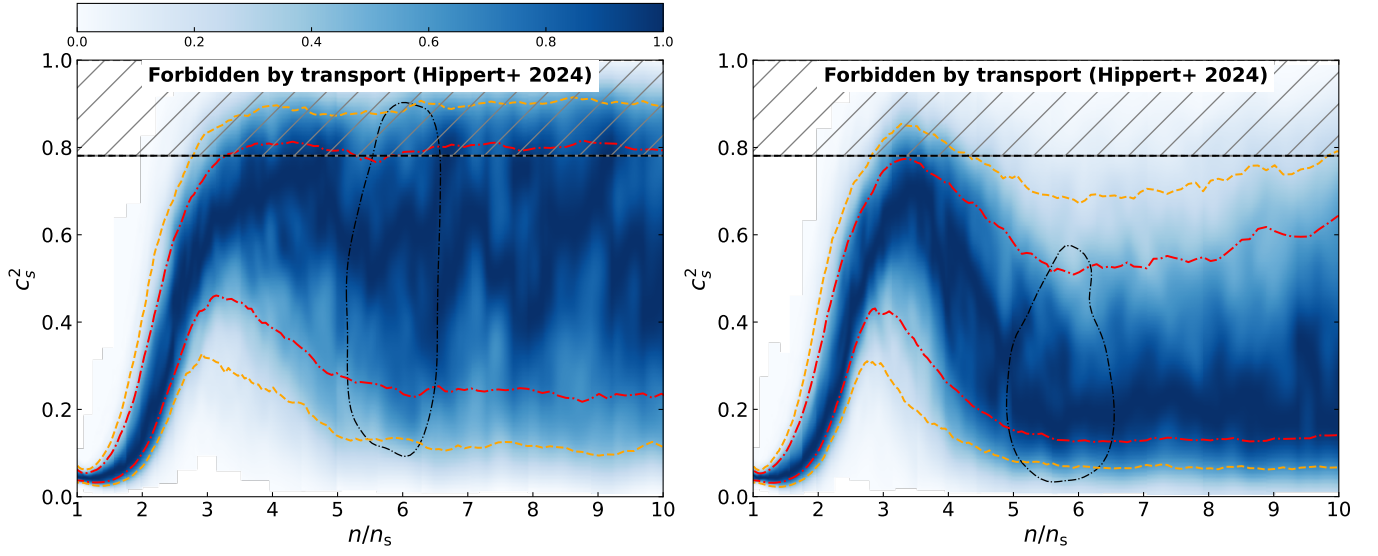


Figure 6. The same as Figure 1, but is derived using $c_s^2 \leq 0.781$ extension of pQCD to lower densities.

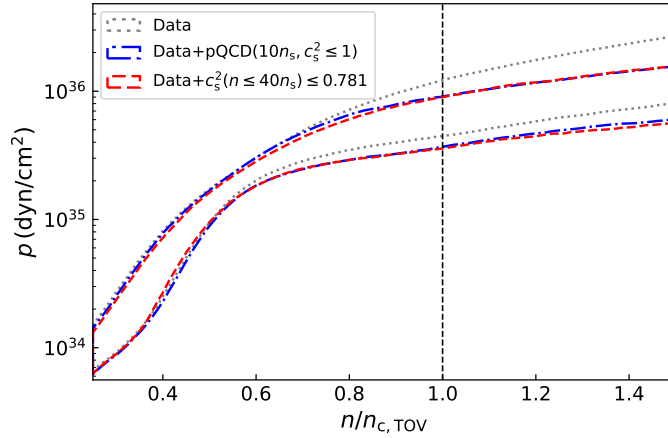


Figure 7. Similar to Figure 2, but is for the pressure versus number density (normalized to $n_{c,\text{TOV}}$) relationship.

and tidal deformability ($\Lambda_{1.4}$) for a canonical $1.4M_\odot$ NS. The inferred $R_{1.4}$ and $\Lambda_{1.4}$ are constrained to $11.94^{+0.77}_{-0.68}$ km and 351^{+195}_{-113} , which are strongly correlated with each other (Malik et al. 2018) since these bulk properties are mainly determined by the pressure at approximately twice the nuclear saturation density ($2n_s$) (Lattimer & Prakash 2016). The inferred radius of a $2M_\odot$ NS ($R_{2.0}$) is constrained to $11.99^{+0.88}_{-0.67}$ km, and the difference between $R_{1.4}$ and $R_{2.0}$ is constrained to $-0.1^{+0.42}_{-0.27}$ km. We also investigate the central number density ($n_{c,\text{TOV}}$), pressure ($p_{c,\text{TOV}}$), polytropic index ($\gamma_{c,\text{TOV}}$), and the squared speed of sound. These central properties are assessed for NSs at their maximum mass configuration ($M = M_{\text{TOV}}$). We notice that there is an intriguing anti-correlation between R_{TOV} and $n_{c,\text{TOV}}$, which was also reported by Jiang et al. (2023). Establishing the criterion for the emergence of strongly coupled conformal matter is crucial for determining the possible existence of a quark core within massive NSs. For instance, the normalized trace anomaly ($\Delta_{c,\text{TOV}} = 1/3 - p_{c,\text{TOV}}/e_{c,\text{TOV}}$), as discussed in Fujimoto et al. (2022), has been suggested as indicative of conformality in NSs. Additionally, a conformal criterion, denoted as $d_{c,\text{TOV}} = \sqrt{\Delta_{c,\text{TOV}}^2 + \Delta'_{c,\text{TOV}}{}^2}$ was proposed by Annala et al. (2023). Besides, Marzenko et al. (2024) argued that the curvature of the energy per particle $\beta_{c,\text{TOV}} = c_{s,\text{TOV}}^2 - 2(1/3 - \Delta_{c,\text{TOV}})/(4/3 - \Delta_{c,\text{TOV}})$ may serve as an approximate order parameter that signifies the

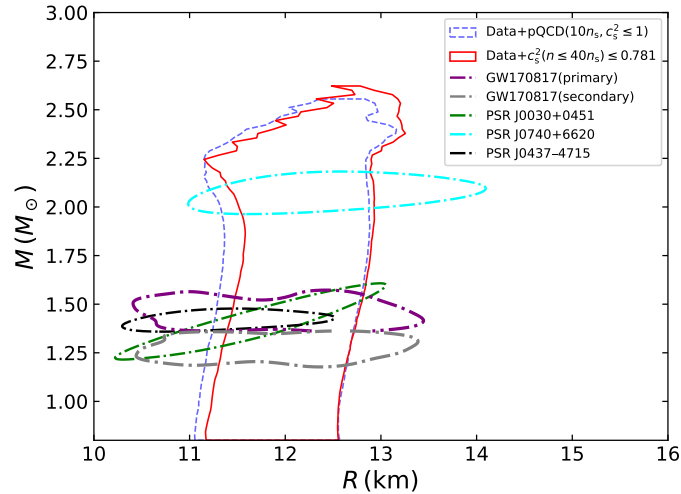


Figure 8. Reconstructed 90% intervals of mass-radius curves. The blue and red lines depict the outcomes derived from multimessenger NS observations when combined with a pQCD constraint applied at a density of $10n_s$, and the outcomes obtained from multimessenger NS observations with the imposition of a transport upper bound on the speed of sound squared $c_s^2 \leq 0.781$, respectively. The green, cyan, purple, grey, and black dash-dotted contours represent the 68.3% mass-radius measurements for PSR J0030+0451 (i.e., the ST+PDT model results reported in Vinciguerra et al. (2024)), the very massive PSR J0740+6620 (Salmi et al. 2024), the primary NS of GW170817, the secondary component of GW170817 (Abbott et al. 2018), and PSR J0437–4715 (Choudhury et al. 2024), respectively.

onset of strongly coupled conformal matter in the NS core. All these parameters are included in the corner plots (i.e., Figure 9).

REFERENCES

- Abbott, B. P., Abbott, R., Abbott, T. D., et al. 2018, *PhRvL*, 121, 161101, doi: [10.1103/PhysRevLett.121.161101](https://doi.org/10.1103/PhysRevLett.121.161101)
- . 2019, *Physical Review X*, 9, 011001, doi: [10.1103/PhysRevX.9.011001](https://doi.org/10.1103/PhysRevX.9.011001)
- Altiparmak, S., Ecker, C., & Rezzolla, L. 2022, *ApJL*, 939, L34, doi: [10.3847/2041-8213/ac9b2a](https://doi.org/10.3847/2041-8213/ac9b2a)
- Annala, E., Gorda, T., Hirvonen, J., et al. 2023, *Nature Communications*, 14, 8451, doi: [10.1038/s41467-023-44051-y](https://doi.org/10.1038/s41467-023-44051-y)
- Annala, E., Gorda, T., Kurkela, A., Nätttilä, J., & Vuorinen, A. 2020, *Nature Physics*, 16, 907, doi: [10.1038/s41567-020-0914-9](https://doi.org/10.1038/s41567-020-0914-9)
- Antoniadis, J., Freire, P. C. C., Wex, N., et al. 2013, *Science*, 340, 448, doi: [10.1126/science.1233232](https://doi.org/10.1126/science.1233232)
- Arnold, P., Moore, G. D., & Yaffe, L. G. 2003, *Journal of High Energy Physics*, 2003, 051, doi: [10.1088/1126-6708/2003/05/051](https://doi.org/10.1088/1126-6708/2003/05/051)
- Baier, R., Romatschke, P., Thanh Son, D., Starinets, A. O., & Stephanov, M. A. 2008, *Journal of High Energy Physics*, 2008, 100, doi: [10.1088/1126-6708/2008/04/100](https://doi.org/10.1088/1126-6708/2008/04/100)
- Bedaque, P., & Steiner, A. W. 2015, *PhRvL*, 114, 031103, doi: [10.1103/PhysRevLett.114.031103](https://doi.org/10.1103/PhysRevLett.114.031103)
- Brandes, L., Weise, W., & Kaiser, N. 2023a, *PhRvD*, 108, 094014, doi: [10.1103/PhysRevD.108.094014](https://doi.org/10.1103/PhysRevD.108.094014)
- . 2023b, *PhRvD*, 107, 014011, doi: [10.1103/PhysRevD.107.014011](https://doi.org/10.1103/PhysRevD.107.014011)
- Choudhury, D., Salmi, T., Vinciguerra, S., et al. 2024, *arXiv e-prints*, arXiv:2407.06789, doi: [10.48550/arXiv.2407.06789](https://doi.org/10.48550/arXiv.2407.06789)
- Dittmann, A. J., Miller, M. C., Lamb, F. K., et al. 2024, *arXiv e-prints*, arXiv:2406.14467, doi: [10.48550/arXiv.2406.14467](https://doi.org/10.48550/arXiv.2406.14467)
- Ecker, C., & Rezzolla, L. 2022, *ApJL*, 939, L35, doi: [10.3847/2041-8213/ac8674](https://doi.org/10.3847/2041-8213/ac8674)
- Essick, R., Landry, P., & Holz, D. E. 2020, *PhRvD*, 101, 063007, doi: [10.1103/PhysRevD.101.063007](https://doi.org/10.1103/PhysRevD.101.063007)
- Essick, R., Legred, I., Chatziioannou, K., Han, S., & Landry, P. 2023, *PhRvD*, 108, 043013, doi: [10.1103/PhysRevD.108.043013](https://doi.org/10.1103/PhysRevD.108.043013)
- Fan, Y.-Z., Han, M.-Z., Jiang, J.-L., Shao, D.-S., & Tang, S.-P. 2024, *PhRvD*, 109, 043052, doi: [10.1103/PhysRevD.109.043052](https://doi.org/10.1103/PhysRevD.109.043052)
- Fonseca, E., Cromartie, H. T., Pennucci, T. T., et al. 2021, *ApJL*, 915, L12, doi: [10.3847/2041-8213/ac03b8](https://doi.org/10.3847/2041-8213/ac03b8)

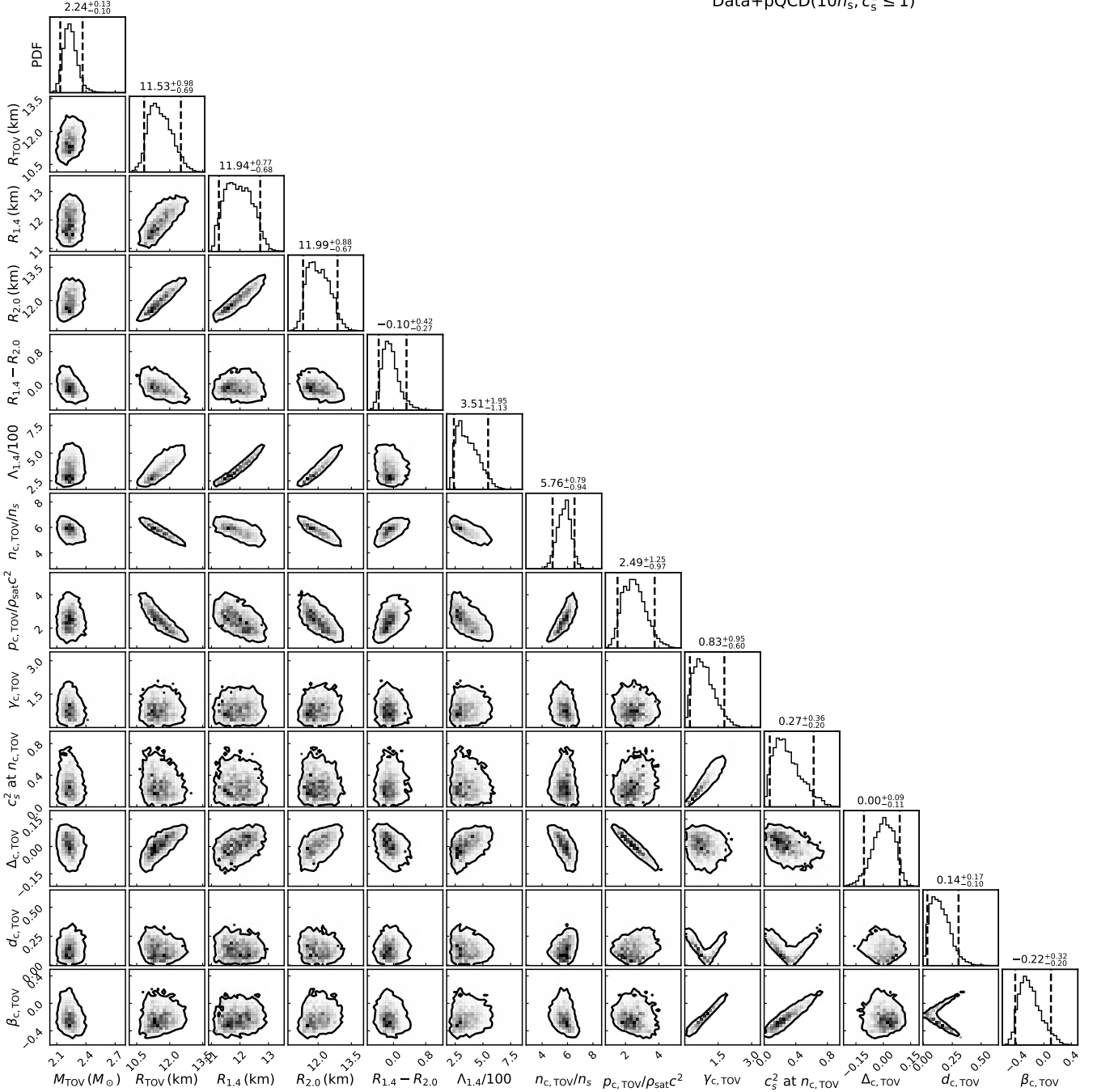
Data+pQCD($10n_s, c_s^2 \leq 1$)

Figure 9. Corner plots of the probability distributions for the maximum mass (M_{TOV}) and corresponding radius (R_{TOV}) of a non-rotating NS, the radius ($R_{1.4}$) and tidal deformability ($\Lambda_{1.4}$) of a canonical $1.4M_\odot$ NS, the radius of a $2M_\odot$ NS ($R_{2.0}$), the difference between $R_{1.4}$ and $R_{2.0}$, and the number density ($n_{c,\text{TOV}}$, normalized to nuclear saturation density n_s), pressure ($p_{c,\text{TOV}}$, normalized to the product of the rest-mass density at n_s and the square of the speed of light c^2), polytropic index ($\gamma_{c,\text{TOV}}$), and the squared sound speed, and the normalized trace anomaly ($\Delta_{c,\text{TOV}}$ Fujimoto et al. (2022)) in the center of the NS with $M = M_{\text{TOV}}$. Additionally, $d_{c,\text{TOV}}$, a conformal criterion introduced by Annala et al. (2023), and $\beta_{c,\text{TOV}}$, representing the curvature of the energy per particle as proposed by Marzenko et al. (2024), are included. All uncertainties are reported at the 90% credible level.

- Fujimoto, Y., Fukushima, K., McLerran, L. D., & Praszalowicz, M. 2022, *PhRvL*, 129, 252702, doi: [10.1103/PhysRevLett.129.252702](https://doi.org/10.1103/PhysRevLett.129.252702)
- Gorda, T., Komoltsev, O., & Kurkela, A. 2023, *ApJ*, 950, 107, doi: [10.3847/1538-4357/acce3a](https://doi.org/10.3847/1538-4357/acce3a)
- Han, M.-Z., Huang, Y.-J., Tang, S.-P., & Fan, Y.-Z. 2023, *Science Bulletin*, 68, 913, doi: [10.1016/j.scib.2023.04.007](https://doi.org/10.1016/j.scib.2023.04.007)
- Hippert, M., Noronha, J., & Romatschke, P. 2024, arXiv e-prints, arXiv:2402.14085, doi: [10.48550/arXiv.2402.14085](https://doi.org/10.48550/arXiv.2402.14085)
- Jiang, J.-L., Ecker, C., & Rezzolla, L. 2023, *ApJ*, 949, 11, doi: [10.3847/1538-4357/acc4be](https://doi.org/10.3847/1538-4357/acc4be)
- Komoltsev, O., & Kurkela, A. 2022, *PhRvL*, 128, 202701, doi: [10.1103/PhysRevLett.128.202701](https://doi.org/10.1103/PhysRevLett.128.202701)
- Komoltsev, O., Somasundaram, R., Gorda, T., et al. 2023, arXiv e-prints, arXiv:2312.14127, doi: [10.48550/arXiv.2312.14127](https://doi.org/10.48550/arXiv.2312.14127)
- Kurkela, A. 2022, arXiv e-prints, arXiv:2211.11414, doi: [10.48550/arXiv.2211.11414](https://doi.org/10.48550/arXiv.2211.11414)
- Landry, P., & Essick, R. 2019, *PhRvD*, 99, 084049, doi: [10.1103/PhysRevD.99.084049](https://doi.org/10.1103/PhysRevD.99.084049)
- Landry, P., Essick, R., & Chatziioannou, K. 2020, *PhRvD*, 101, 123007, doi: [10.1103/PhysRevD.101.123007](https://doi.org/10.1103/PhysRevD.101.123007)
- Lattimer, J. M., & Prakash, M. 2016, *PhR*, 621, 127, doi: [10.1016/j.physrep.2015.12.005](https://doi.org/10.1016/j.physrep.2015.12.005)
- Luo, C.-N., Tang, S.-P., Han, M.-Z., et al. 2024, *ApJ*, 966, 98, doi: [10.3847/1538-4357/ad39ed](https://doi.org/10.3847/1538-4357/ad39ed)
- Malik, T., Alam, N., Fortin, M., et al. 2018, *PhRvC*, 98, 035804, doi: [10.1103/PhysRevC.98.035804](https://doi.org/10.1103/PhysRevC.98.035804)
- Marczenko, M., Redlich, K., & Sasaki, C. 2024, *PhRvD*, 109, L041302, doi: [10.1103/PhysRevD.109.L041302](https://doi.org/10.1103/PhysRevD.109.L041302)
- Miller, M. C., Lamb, F. K., Dittmann, A. J., et al. 2019, *ApJL*, 887, L24, doi: [10.3847/2041-8213/ab50c5](https://doi.org/10.3847/2041-8213/ab50c5)
- Moore, G. D. 2024, arXiv e-prints, arXiv:2404.01968, doi: [10.48550/arXiv.2404.01968](https://doi.org/10.48550/arXiv.2404.01968)
- Moore, G. D., & Sohrabi, K. A. 2012, *Journal of High Energy Physics*, 2012, 148, doi: [10.1007/JHEP11\(2012\)148](https://doi.org/10.1007/JHEP11(2012)148)
- Mroczek, D., Miller, M. C., Noronha-Hostler, J., & Yunes, N. 2023, arXiv e-prints, arXiv:2309.02345, doi: [10.48550/arXiv.2309.02345](https://doi.org/10.48550/arXiv.2309.02345)
- Policastro, G., Son, D. T., & Starinets, A. O. 2001, *PhRvL*, 87, 081601, doi: [10.1103/PhysRevLett.87.081601](https://doi.org/10.1103/PhysRevLett.87.081601)
- Reed, B., & Horowitz, C. J. 2020, *PhRvC*, 101, 045803, doi: [10.1103/PhysRevC.101.045803](https://doi.org/10.1103/PhysRevC.101.045803)
- Riley, T. E., Watts, A. L., Bogdanov, S., et al. 2019, *ApJL*, 887, L21, doi: [10.3847/2041-8213/ab481c](https://doi.org/10.3847/2041-8213/ab481c)
- Romatschke, P., & Romatschke, U. 2007, *PhRvL*, 99, 172301, doi: [10.1103/PhysRevLett.99.172301](https://doi.org/10.1103/PhysRevLett.99.172301)
- . 2017, arXiv e-prints, arXiv:1712.05815, doi: [10.48550/arXiv.1712.05815](https://doi.org/10.48550/arXiv.1712.05815)
- Salmi, T., Choudhury, D., Kini, Y., et al. 2024, arXiv e-prints, arXiv:2406.14466, doi: [10.48550/arXiv.2406.14466](https://doi.org/10.48550/arXiv.2406.14466)
- Somasundaram, R., Tews, I., & Margueron, J. 2023, *PhRvC*, 107, L052801, doi: [10.1103/PhysRevC.107.L052801](https://doi.org/10.1103/PhysRevC.107.L052801)
- Tang, S.-P., Han, M.-Z., Huang, Y.-J., Fan, Y.-Z., & Wei, D.-M. 2024, *PhRvD*, 109, 083037, doi: [10.1103/PhysRevD.109.083037](https://doi.org/10.1103/PhysRevD.109.083037)
- Vinciguerra, S., Salmi, T., Watts, A. L., et al. 2024, *ApJ*, 961, 62, doi: [10.3847/1538-4357/acfb83](https://doi.org/10.3847/1538-4357/acfb83)
- Vuorinen, A. 2024, *Acta Physica Polonica B*, 55, 1, doi: [10.5506/APhysPolB.55.4-A4](https://doi.org/10.5506/APhysPolB.55.4-A4)
- Yao, N., Sorensen, A., Dexheimer, V., & Noronha-Hostler, J. 2023, arXiv e-prints, arXiv:2311.18819, doi: [10.48550/arXiv.2311.18819](https://doi.org/10.48550/arXiv.2311.18819)
- Zhou, D. 2023, arXiv e-prints, arXiv:2307.11125, doi: [10.48550/arXiv.2307.11125](https://doi.org/10.48550/arXiv.2307.11125)